*bioresources.com*

# Activated Carbon Monolith Derived from Polymer and Fast Pyrolytic Char: Effect of Bio-Oil Phenol-Formaldehyde Resin

Lufei Li,[a] Jianmin Chang,[a,*] Liping Cai,[b] and Sheldon Q. Shi [b]

Activated carbon monoliths (ACMs) were fabricated by $H_2O$ activation using powdered fast pyrolytic char (PFPC) as a raw material and bio-oil phenol-formaldehyde (BPF) resin as a binder. The effects of the ratio of BPF resin to PFPC on textural and chemical-surface properties of the ACMs were investigated using elemental analysis, X-ray diffraction (XRD), Fourier transform infrared spectroscopy (FT-IR), and field-emission scanning electron microscopy (FE-SEM). The adsorption capacity and mechanical properties under different conditions were examined by $N_2$ adsorption analysis and compression strength, respectively. The results indicated that the optimal ratio was 20 wt.% BPF resin binder. The compression strength of ACMs with a carbon content of 79.7 wt.% reached 3.74 MPa, while the BET surface area and total pore volume were 731.3 $m^2/g$ and 0.589 $cm^3/g$, respectively. ACMs appeared to be mainly mesoporous with low graphitization and contained multiple functional groups such as alkyl, esters, ether, phenol, olefin, *etc.*

*Keywords: Bio-oil phenol-formaldehyde; Fast pyrolytic char; Activated carbon monoliths*

*Contact information: a: College of Materials Science and Technology, Beijing Forestry University, Beijing, 100083, China; b: Mechanical and Energy Engineering Department, University of North Texas, 3940 N. Elm, Denton, TX, USA; *Corresponding author: cjianmin@bjfu.edu.cn*

## INTRODUCTION

Fast pyrolysis is an effective method to convert biomass to bioenergy due to its eco-friendly and efficient technology. As one of the major products generated by biomass fast pyrolysis, powdered fast pyrolytic char (PFPC) has expansive application prospects due to its high carbon content, particle uniformity, low ash content, and certain pore structure. However, it is commonly used in kilns and boilers as high-heating-value solid fuel, leading to a low utilization value. Thus, there is a need to develop new methods for obtaining high value-added materials from PFPC.

Activated carbon monoliths (ACMs) have the combined advantages of activated carbons (*i.e.*, stability in acidic and alkaline media, high surface area, developed porosity, *etc.*) and monolithic structures (*i.e.*, high strength, high bulk density, no dust pollution, *etc.*), which can be widely used for adsorption, purification, natural gas adsorption storage, catalyst support, and other applications (Liu *et al.* 2007; Inagaki *et al.* 2015). ACMs are typically made from activated carbon and other carbonaceous materials such as coal, petroleum coke, polymeric precursors, and biomass materials (Inagaki *et al.* 2004; Chen *et al.* 2006; Saeidi and Lotfollahi 2015; Arami-Niya *et al.* 2016). Using renewable biomass such as wood, coconut shells, and nut shells, as the feedstock for low-cost and environmentally friendly production has been widely investigated. PFPC is a particularly promising material to produce ACMs due to its good physical properties, low-cost, and ease of processing.

Different approaches have been used to produce ACMs. Binder addition is the conventional method to keep carbonaceous materials compressed with the appropriate mechanical strength (Liu *et al.* 2007; Saeidi and Lotfollahi 2015, 2016). The binder commonly used for molding is humic acid and its sodium salt, coal tar pitch, organic materials, or mixtures of organic and inorganic binders (Liu *et al.* 2007; Gatica *et al.* 2010; Lim *et al.* 2010; Saeidi and Lotfollahi 2015). As a poly-condensation product of phenol and formaldehyde, phenol-formaldehyde (PF) resin is one of the most advantageous binders due to its high char yield, good mechanical properties, and low micropore blocking of ACMs (Lozano-Castello´ *et al.* 2002; Yi *et al.* 2012). However, the utilization of PF is currently limited due to the high cost and the dependence on non-renewable resources (95% of phenol is sourced from petroleum), which drives researchers to find an effective modification to reduce the amount of petrochemical in phenol without compromising its performance advantages (Yi *et al.* 2012). Bio-oil is obtained from biomass fast pyrolysis. Because it is rich in phenolic compounds, it can be used as a potential phenolic substance to synthesize bio-oil phenol-formaldehyde (BPF) resins, which could reduce costs and ensure high-efficiency utilization (Fan *et al.* 2010; Yi *et al.* 2012).

To improve the physicochemical properties, the physical activation with steam is one of the well-known activation methods of activated carbons (Pastor-Villegas and Duran-Valle 2002; Bouchelta *et al.* 2008). This method grants ACMs with a high surface area and a developed porosity to meet the requirements of each application. In this study, the ACMs produced using BPF resin as a binder and PFPC as the raw material were pressed into pillars. The carbon pillars were activated by steam. The influence of the ratio of BPF to PFPC on chemical-surface properties, adsorption capacity, and mechanical properties of the resultant ACMs was investigated to obtain the optimal production parameters.

## EXPERIMENTAL

### Materials

The PFPC was produced by the fast pyrolysis of pine sawdust at the Institute of Wood Based Material, Beijing Forestry University, Beijing, China. Preparation of PFPC was conducted by the fast pyrolyzing of pine sawdust sized 0.45-0.9 mm in diameter at about 500 °C in a fluidized-bed for 1-2 s. Its BET surface area and total pore volume were 10.12 $m^2$/g and 0.0178 $cm^3$/g, respectively. Table 1 presents the proximate and elemental analyses results of the PFPC used in this study.

**Table 1.** Proximate and Elemental Analysis of PFPC

| Materials | Proximate analysis (wt.%) | | | | Elemental analysis (wt.%) | | | |
|---|---|---|---|---|---|---|---|---|
| | $M_{ad}$ | $V_{ad}$ | $FC_{ad}$ | $A_{ad}$ | C | H | N | S |
| PFPC | 4.01 | 21.25 | 69.17 | 9.58 | 72.44 | 3.24 | 0.22 | n.d. |

ad, air-dried; n.d., not detected

BPF resin was supplied by the Institute of Wood Based Material, Beijing Forestry University, Beijing, China. It had a black and sticky appearance with a viscosity of 488 mPa•s and a solids content of 50.8%.

## Methods

*Preparation of the ACMs from PFPC and BPF*

The PFPC was obtained from a series of high temperature pyrolysis treatments using *Pinus sylvestris* var. *mongolica* Litv. sawdust as the feedstock. Various amounts of BPF resin were added to the PFPC and then mixed mechanically at room temperature. The mixture of PFPC and BPF resin was molded under a pressure of 20 MPa into a monolith at 120 °C (the BPF resin curing temperature). The monolith was then activated by steaming to obtain the ACMs. The activation conditions used were based on the previous results for producing monolith with the most suitable porous texture and mechanical properties. The monolith was activated at 800 °C for 1 h in a $H_2O$ flow of 600 mL/min with a controlled heating rate of 10 °C/min.

A series of ACMs were prepared using the bio-oil phenol-formaldehyde amounts of 10, 20, 30, 40, and 50 wt.% (wt.% of PFPC). The ACMs were designated ACM-10%, ACM-20%, ACM-30%, ACM-40%, and ACM-50% for the sake of convenience.

*Elemental analysis*

Elemental analysis (EA) of the ACMs was conducted on an Elementar Vario EL III elemental analyzer (Elementar, Langenselbold, Germany).

*Fourier transform infrared spectroscopy (FTIR) analysis*

To characterize the ACM's functional groups, Fourier transform infrared spectroscopy was conducted using a Vertex 70 FTIR spectrometer (Bruker, Karlsruhe, Baden Wurttemberg, Germany) in absorbance mode. The spectra were obtained in the range of 4000 to 400 $cm^{-1}$ with a resolution of 4 $cm^{-1}$ and 32 scans.

*X-ray diffraction (XRD) analysis*

The crystal structure of the ACMs was examined by X-ray diffraction in the $2\theta$ range of 3° to 80° using a Smartlab-3kW system (Rigaku, Tokyo, Japan) with a scanning speed of 3°/min.

*$N_2$ adsorption analysis*

Surface areas of the ACMs were determined according to the BET (Emmett and Teller, Brunauer) equation, using nitrogen adsorption measurements at 77 K in an Autosorb 3-B volumetric system (Quantachrome, Boynton Beach, FL, USA). The mesoporous size distributions were calculated using the BJH (Barrett–Joyner–Halenda) method (Jacques *et al.* 2007), respectively.

*Compression strength*

The compression strength of the ACMs was measured using a universal material testing machine (Z005, Zwick/Roell, Ulm, Germany) under a loading speed of 1 mm/min. The compression strength, *P*, was calculated using Eq. 1,

$$P = F/S \tag{1}$$

where *F* is the load at failure and *S* is the cross-sectional area of the monolith. The data presented in this paper were typically an average of three measurements.

*Scanning electron microscope (SEM)*

The microstructures of ACMs were observed using a scanning electron microscope (Hitachi SU8010, Tokyo, Japan)). Images were obtained at 5000 V excitation energy.

## RESULTS AND DISCUSSION

### Proximate and Ultimate Analysis

Table 2 summarizes the results of elemental analyses of the ACMs. The ACMs had high carbon contents but contained no sulphur, which had a positive impact on pyrolytic char due to the improved quality of the ACMs. The elemental content of the samples changed with the binder ratio. When the ratio of BPF to PFPC increased from 10 wt.% to 30 wt.%, the carbon contents of the ACMs increased from 78.9 wt.% to 82.2 wt.% and then decreased to 79.8 wt.% when the BPF/PFPC ratio increased to 50 wt.%. The hydrogen contents changed between 0.93 wt.% and 1.10 wt.% at different process conditions. At different treatment conditions, the carbon contents of the samples increased and the hydrogen contents decreased compared to PFPC. This result was attributed to the release of volatiles during activation, resulting in the elimination of non-carbon species and the enrichment of carbon (Aygün *et al.* 2003).

The product yield is an important measure of the feasibility of preparing activated carbon from a given precursor (Angın *et al.* 2013). Table 2 presents the product yields of samples obtained at different BPF/PFPC ratios. The yields of samples ranged from 57 wt.% to 64 wt.%. As the BPF/PFPC ratio increased, the yields of the ACMs showed a tendency to first increase and then decrease. The maximum value was obtained at a BPF/PFPC ratio of 20 wt.%.

**Table 2.** Elemental Content and Yield of ACMs

| Sample | C (wt.%) | H (wt.%) | N (wt.%) | S (wt.%) | Yield (wt.%) |
|--------|----------|----------|----------|----------|--------------|
| ACM-10% | 78.89 | 1.10 | 0.16 | n.d. | 63 |
| ACM-20% | 79.66 | 0.93 | 0.16 | n.d. | 64 |
| ACM-30% | 82.21 | 0.96 | 0.16 | n.d. | 61 |
| ACM-40% | 81.00 | 0.97 | 0.17 | n.d. | 58 |
| ACM-50% | 79.83 | 1.01 | 0.16 | n.d. | 57 |

n.d., not detected

### FTIR Analysis

The chemical reactivity of functional groups on the surface was investigated using FTIR, which gives insight to the adsorption capability of ACMs. The FTIR spectra of the ACMs obtained at different BPF/PFPC ratios are shown in Fig. 1. The FTIR spectra of the different samples were similar, with a band at about 3408 $cm^{-1}$ due to the -OH stretching vibration in hydroxyl groups or adsorbed water (Wu *et al.* 2011). The small, weak bands that appear at about 2918 $cm^{-1}$ and 2851 $cm^{-1}$ are generally due to C-H stretching vibrations (Li *et al.* 2011; Wu *et al.* 2011). The weak bands located at 1636 $cm^{-1}$ are characteristic peaks of the carboxylate group, which were possibly formed due to the extraction of hydrogen and OH groups from the aromatic rings during the dehydration process in the heat treatment stages by the releasing of $H_2O$ molecule (Somasundaram *et al.* 2013). According to previous studies, the PFPC was rich in OH groups which decreased after activation (Han *et al.* 2013). The bands at 1558 $cm^{-1}$ and 1429 $cm^{-1}$ could be assigned to

C=C groups from aromatics and alkyl groups, respectively (de Souza Macedo *et al.* 2006; Foo and Hameed 2011). The band became weak when increasing the BPF/PFPC ratio from 10 wt.% to 30 wt.% and then slightly intensified when the BPF/PFPC ratio increased from 30 wt.% to 50 wt.%. The band at 1076 cm$^{-1}$ is a characteristic peak of the C–O–C group (Foo and Hameed 2011). The peak at 876 cm$^{-1}$ could be indicative of the presence of a C-H group (Zhang *et al.* 2015). The intensities of the bands changed with varying BPF/PFPC ratios, indicating that functional groups are affected by the BPF/PFPC ratio. However, producing ACMs by varying the BPF/PFPC ratio did not modify the functional groups at the surface. The FTIR analyses suggested that the existence of multiple functional groups (alkyl, esters, ether, phenol, olefin, *etc*.) on the surface of the ACMs provided samples with adsorption capacity and catalysis ability (Ma *et al.* 2012).
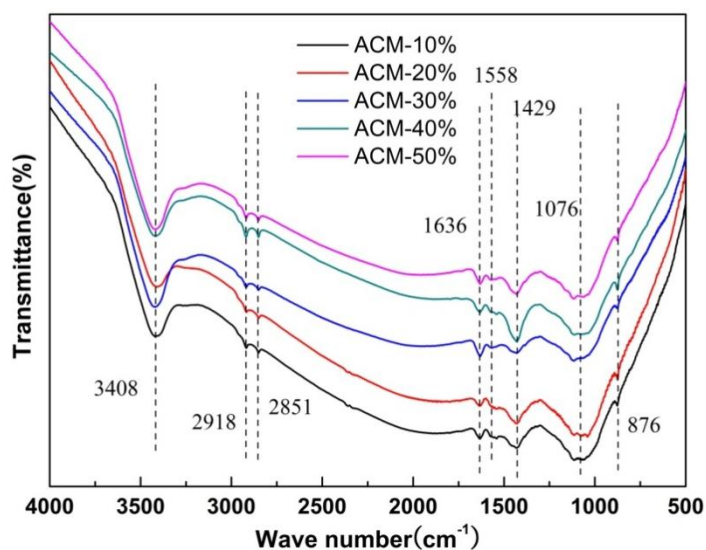


**Fig. 1.** FTIR spectra of ACMs at different BPF/PFPC ratios
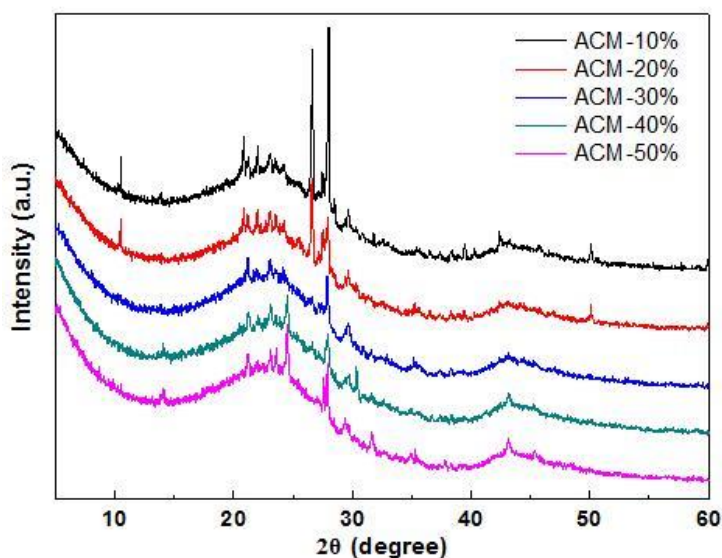


**Fig. 2.** XRD patterns of ACMs at different BPF/PFPC ratios

### X-ray Diffraction Analysis

The crystal structure of the ACMs was investigated using XRD. The typical XRD patterns of the ACMs obtained at different process conditions are shown in Fig. 2. A broad and obvious diffraction peak (002) appeared in the range $2\theta = 20°$ to $30°$, indicating the preservation of several amorphous compounds (Liu *et al.* 2013). The samples showed a (100/101) peak near 43° due to the graphitic structure (Yang *et al.* 2014). The XRD patterns of different samples changed with the BPF/PFPC ratio. The intense diffraction peaks at $2\theta = 26.6°$, known as a small graphite-like structure, decreased gradually until almost disappearing with increasing BPF ratio (Azargohar and Dalai 2006). The diffraction peaks near 28° also showed a similar trend. This may be due to the possibility that BPF could not form the graphite structure during the activation process, which caused the crystal structure of the samples to change after increasing the amount of binder.
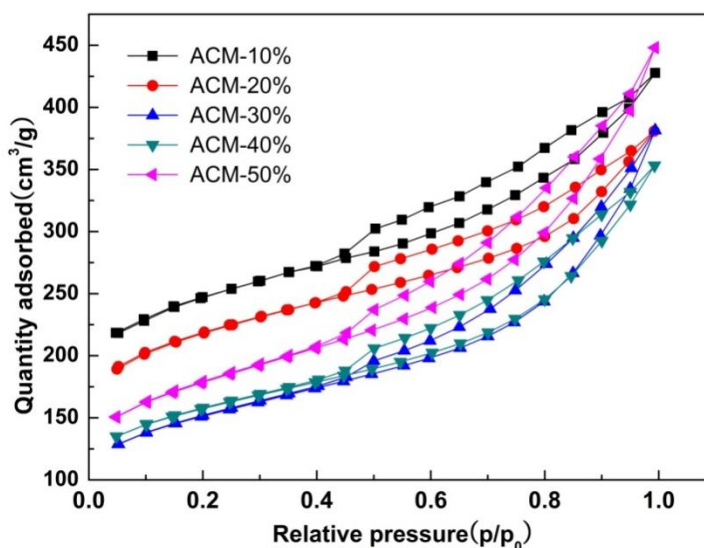


**Fig. 3.** $N_2$ adsorption-desorption isotherms of ACMs at different BPF/PFPC ratios

### $N_2$ Adsorption-Desorption Analysis

Figure 3 presents the nitrogen adsorption-desorption isotherms of the activated carbon monoliths prepared with different BPF/PFPC ratios. The preliminary qualitative information from the samples can be provided by the shape of curve. According to IUPAC classification, the curves of these ACMs exhibited a type IV shape with a characteristic H4-type hysteresis loop for mesoporous materials. Each isotherm of the ACMs showed a plateau at high relative pressures toward the end of the curves, indicating capillary condensation of liquid $N_2$ in the mesopores or macropores. The figure shows that the adsorption capacity of the samples first decreased when the BPF/PFPC ratio increased from 10 wt.% to 30 wt.% and then increased with an increase in the BPF/PFPC ratio from 30 wt.% to 50 wt.%. Textural characteristics of ACMs according to different BPF/PFPC ratios are shown in Table 3. The specific surface area, mesopore surface, and volume of ACMs firstly decreased and then increased as the BPF/PFPC ratio increased. It was indicated that the addition of binder to PFPC was averse to forming pores in the preparation process. This fact can be due to the space that the BPF occupied and the porosity that it blocked. On the other hand, excess binder resulted in an increase in the number of pores. The BPF resin dispersed around the PFPC in the mixing and molding process. With the increase of

*bioresources*.com

BPF/PFPC ratio, the shrinkage ratio of monoliths grew in the activation process which enabled some çed pores exposed.

**Table 3.** Textural Characteristics of ACMs

| Samples | $S_{BET}(m^2/g)$ | $S_{meso}(m^2/g)$ | $V_{tot}(cm^3/g)$ | $V_{meso}(cm^3/g)$ |
|---|---|---|---|---|
| ACM-10% | 823.91 | 467.10 | 0.6476 | 0.436 |
| ACM-20% | 731.30 | 423.96 | 0.5892 | 0.432 |
| ACM-30% | 513.29 | 328.97 | 0.5462 | 0.409 |
| ACM-40% | 531.02 | 346.61 | 0.5900 | 0.488 |
| ACM-50% | 606.68 | 408.44 | 0.6947 | 0.579 |

**Compression Strength Analysis**

Figure 4 depicts the effect of the BPF/PFPC ratio on the compression strength of the activated carbon monoliths. As the BPF/PFPC ratio increased, the compression strength tended to first increase and then decrease. Increasing the BPF/PFPC ratio up to 30 wt.% led to a rise in the compression strength. The compression strength reached its highest when the BPF/PFPC ratio was 30 wt.%. Above this ratio, the higher the binder content in the monolith, the lower the compression strength. The addition of binder is beneficial for molding the powdered PFPC. When the amount of binder is too small, the monoliths are not sufficiently wetted, resulting in inadequate mechanical properties. Increasing the binder content promotes further wetting which increases adhesion between the binder and PFPC, leading to an increase in bonding stability of the mixed material. The liquid content of the mixture increased with the future increase in the BPF/PFPC ratio, resulting in reduced contact between the carbon particles. When the BPF activated in high temperatures, it swelled, leading to a loose structure and a reduction in mechanical properties. This explains the strength degradation behavior above a 30 wt.% BPF/PFPC ratio. As shown in Fig. 4, the compression strength of ACM-10% was too small to meet application requirements. Considering adsorptive properties, mechanical properties, and product costs, the optimum PBF/PFPC ratio was 20 wt.%.
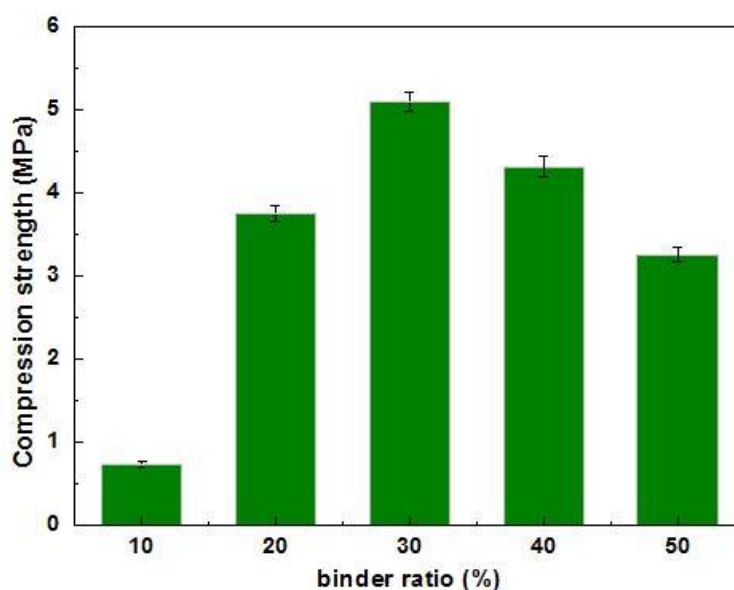


**Fig. 4.** Compression strength of ACMs at different BPF/PFPC ratios

### SEM Analysis

Figure 5 shows SEM images of the activated carbon monoliths molded with a BPF/PFPC ratio of 20 wt.%. Figures 5(A), 5(B), and 5(C) present the cases of 5.00 K, 45.0 K, and 90.0 K magnification, respectively. The existence states of BPF in the structure of ACMs are shown in Fig. 5. The carbonized BPF resin attached to the surface of the activated carbon particles, which gave the samples adequate mechanical properties. However, its presence led to pore clogging. In Figs. 5 (B) and (C), the presence of many mesopores and macropores on the particle surface can be observed, which were primarily created through the heating and encroachment by $H_2O$. The pyrolysis of BPF and the release of volatile components may be another contributing factor affecting the creation of pores in the ACMs. The presence of pores played an outstanding role in adsorption.



|  (A)  |  (B)  |  (C)  |
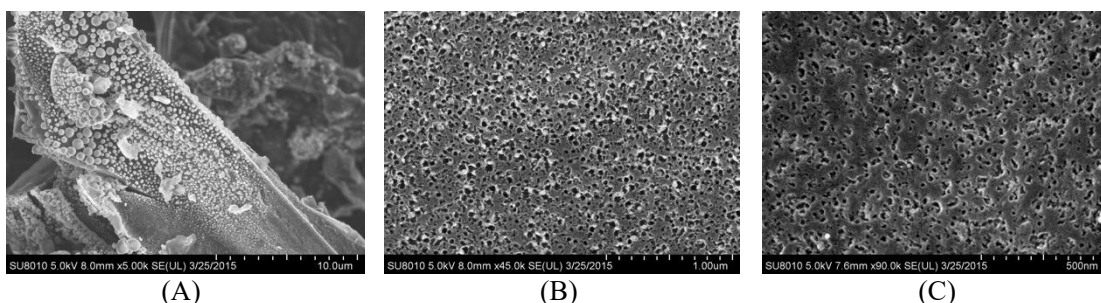
**Fig. 5.** Scanning electron microscope photographs of ACM-20% at 5.00 K (A), 45.00 K (B), and 90.00 K (C)

### CONCLUSIONS

1. ACMs with developed pore structures were prepared using PFPC as a raw material and BPF resin as a binder. The adjustment of the ratio of BPF to PFPC was an effective method to stabilize the monoliths. Multiple functional groups (alkyl, esters, ether, phenol, olefin, *etc*.) were formed on the surface of ACMs, which appeared to be mainly mesoporous with low graphitization.

2. The optimal ratio was 20 wt.% PBF/PFPC. At this condition, the BET surface area and total pore volume of the ACM with a carbon content 79.7 wt.% were 731.3 $m^2$/g and 0.589 $cm^3$/g, respectively, while the compression strength reached 3.74 MPa.

3. The availability of the raw materials, multiple surface functionalities, efficient adsorption properties, stability of the monolithic structure, and cost effectiveness offer the ACMs great potential to be used as block adsorbents in the waste treatment industry.

### ACKNOWLEDGMENTS

*bioresources*.com

## REFERENCES CITED

Angın, D., Altintig, E., and Köse, T. E. (2013). "Influence of process parameters on the surface and chemical properties of activated carbon obtained from biochar by chemical activation," *Bioresource Technology* 148(11), 542-549. DOI: 10.1016/j.biortech.2013.08.164

Arami-Niya, A., Rufford, T. E., and Zhu, Z. (2016). "Activated carbon monoliths with hierarchical pore structure from tar pitch and coal powder for the adsorption of $CO_2$, $CH_4$ and $N_2$," *Carbon* 103, 115-124. DOI: 10.1016/j.carbon.2016.02.098

Aygüna, A., Yenisoy-Karakaş, S., and Duman, I. (2003). "Production of granular activated carbon from fruit stones and nutshells and evaluation of their physical, chemical and adsorption properties," *Microporous and Mesoporous Materials* 66(2-3), 189-195. DOI: 10.1016/j.micromeso.2003.08.028

Azargohar, R., and Dalai, A. K. (2006). "Biochar as a precursor of activated carbon," *Applied Biochemistry and Biotechnology* 131(1–3), 762-773. DOI: 10.1007/978-1-59745-268-7_62

Bouchelta, C., Medjram, M. S., Bertrand, O., and Bellat, J. P. (2008). "Preparation and characterization of activated carbon from date stones by physical activation with steam," *Journal of Analytical and Applied Pyrolysis* 82(1), 70-77. DOI: 10.1016/j.jaap.2007.12.009

Chen, C., Kennel, E. B., Stiller, A. H., Stansberry, P. G., and Zondlo, J. W. (2006). "Carbon foam derived from various precursors," *Carbon* 44 (8), 1535-1543. DOI: 10.1016/j.carbon.2005.12.021

de Souza Macedo, J., da Costa Júnior, N. B., Almeida, L. E., da Silva Vieira, E. F., Cestari, A. R., de Fátima Gimenez, I., Villarreal Carreño, N. L., and Barreto, L. S. (2006). "Kinetic and calorimetric study of the adsorption of dyes on mesoporous activated carbon prepared from coconut coir dust," *Journal of Colloid and Interface Science* 298(2), 515-522. DOI: 10.1016/j.jcis.2006.01.021

Fan, D., Chang, J., Gou, J., Xia, B., and Ren, X. (2010). "On the cure acceleration of oil-phenol-formaldehyde resins with different catalysts," *The Journal of Adhesion* 86(8), 836-845. DOI: 10.1080/00218464.2010.498730

Foo, K. Y., and Hameed, B. H. (2011). "Microwave-assisted preparation of oil palm fiber activated carbon for methylene blue adsorption," *Chemical Engineering Journal* 166(2), 792-795. DOI: 10.1016/j.cej.2010.11.019

Gatica, J. M., Harti, S., and Vidal, H. (2010). "Changing the adsorption capacity of coal-based honeycomb monoliths for pollutant removal from liquid streams by controlling their porosity," *Applied Surface Science* 256(23), 7111-7117. DOI: 10.1016/j.apsusc.2010.05.036

Han, Y., Boateng, A. A., Qi, P. X., Lima, I. M., and Chang, J. (2013). "Heavy metal and phenol adsorptive properties of biochars from pyrolyzed switchgrass and woody biomass in correlation with surface properties," *Journal of Environmental Management* 118, 196-204. DOI: 10.1016/j.jenvman.2013.01.001

Inagaki, M., Morishita, T., Kuno, A., Kito, T., Hirano, M., Suwa, T., and Kusakawa, K. (2004). "Carbon foams prepared from polyimide using urethane foam template," *Carbon* 42(3), 497-502. DOI: 10.1016/j.carbon.2003.12.080

Inagaki, M., Qiu, J., and Guo, Q. (2015). "Carbon foam: Preparation and application," *Carbon* 87, 128-152. DOI: 10.1016/j.carbon.2015.02.021

**bioresources.com**

Jacques, R. A., Bernardi, R., Caovila, M., Lima, E. C., Pavan, F. A., Vaghetti, J. C. P., and Airoldi, C. (2007). "Removal of Cu(II), Fe(III) and Cr(III) from aqueous solution by aniline grafted silica gel," *Separation Science and Technology* 42(3), 591-609. DOI: 10.1080/01496390601069952

Li, M., Li, W., and Liu, S. (2011). "Hydrothermal synthesis, characterization, and KOH activation of carbon spheres from glucose," *Carbohydrate Research* 346(8), 999-1004. DOI: 10.1016/j.carres.2011.03.020

Lim, J. W., Choi, Y., Yoon, H. S., Park, Y. K., Yim, J. H., and Jeon, J. K. (2010). "Extrusion of honeycomb monoliths employed with activated carbon-LDPE hybrid materials," *Journal of Industrial and Engineering Chemistry* 16(1), 51-56. DOI: 10.1016/j.jiec.2010.01.022

Liu, L., Liu, Z., Yang, J., Huang, Z., and Liu, Z. (2007). "Effect of preparation conditions on the properties of a coal-derived activated carbon honeycomb monolith," *Carbon* 45(14), 2836-2842. DOI: 10.1016/j.carbon.2007.08.006

Liu, Y., Cai, Q., Li, H., and Zhang, J. (2013). "Fabrication and characterization of mesoporous carbon nanosheets using halloysite nanotubes and polypyrrole *via* a template-like method," *Journal of Applied Polymer Science* 128(1), 517-512. DOI: 10.1002/app.38208

Lozano-Castelló, D., Cazorla-Amorós, D., Linares-Solano, A., and Quinn, D. F. (2002). "Activated carbon monoliths for methane storage: Influence of binder," *Carbon* 40(15), 2817-2825. DOI: 10.1016/S0008-6223(02)00194-X

Ma, C. Y., Xiong, H. Z., and Song, X. S. (2012). "Preparation and characterization of eggplant stalk activated carbon by zinc chloride," *Journal of Functional Materials* 43(3), 342-345. DOI: 10.1016/j.fuproc.2014.04.002

Pastor-Villegas, J., and Duran-Valle, C. J. (2002). "Pore structure of activated carbons prepared by carbon dioxide and steam activation at different temperatures from extracted rockrose," *Carbon* 40(3), 397-402. DOI: 10.1016/S0008-6223(01)00118-X

Saeidi, N., and Lotfollahi, M. N. (2015). "A procedure to form powder activated carbon into activated carbon monolith," *The International Journal of Advanced Manufacturing Technology* 81(5), 1281-1288. DOI: 10.1007/s00170-015-7311-z

Saeidi, N., and Lotfollahi, M. N. (2016). "Effects of powder activated carbon particle size on activated carbon monoliths properties," *Materials and Manufacturing Processes* 16 (12), 543-549. DOI: 10.1080/10426914.2015.1117630

Somasundaram, S., Sekar, K., Gupta, V. K., and Ganesan, S. (2013). "Synthesis and characterization of mesoporous activated carbon from rice husk for adsorption of glycine from alcohol-aqueous mixture," *Journal of Molecular Liquids* 177(10), 416-425. DOI: 10.1016/j.molliq.2012.09.022

Wu, X., Zhu, W., Zhang, X., Chen, T., and Frost, R. L. (2011). "Catalytic deposition of nanocarbon onto palygorskite and its adsorption of phenol," *Applied Clay Science* 52(4), 400-406. DOI: 10.1016/j.molliq.2012.09.022

Yang, C. S., Jang, Y. S., and Jeong, H. K. (2014). "Bamboo-based activated carbon for supercapacitor applications," *Current Applied Physi*cs 14(12), 1616-1620. DOI: 10.1016/j.cap.2014.09.021

Yi, J., Zhang, J., Yao, S., Chang, J., and Li, B. (2012). "Preparation of bio-oil-phenol-formaldehyde resins from biomass pyrolysis oil," *Applied Mechanics and Materials* 174-177, 1429-1432. DOI: 10.4028/www.scientific.net/AMM.174-177.1429

Zhang, G., Shi, L., Zhang, Y., Wei, D., Yan, T., Wei, Q., and Du, B. (2015). "Aerobic granular sludge-derived activated carbon mineral acid modification and superior dye adsorption capacity," *RSC Advances* 5(32), 25279-25286. DOI: 10.1039/C4RA15216F